Atmos. Meas. Tech. Discuss., 7, 9537–9571, 2014
www.atmos-meas-tech-discuss.net/7/9537/2014/
doi:10.5194/amtd-7-9537-2014

Atmospheric Measurement Techniques Discussions
Open Access

Using digital image processing to characterize the Campbell–Stokes sunshine recorder and to derive high-temporal resolution direct solar irradiance

A. Sanchez-Romero, J. A. González, J. Calbó, and A. Sanchez-Lorenzo

Department of Physics, University of Girona, Girona, Spain

Received: 30 July 2014 – Accepted: 31 August 2014 – Published: 17 September 2014

Correspondence to: A. Sanchez-Romero (alejandro.sanchez@udg.edu)

Published by Copernicus Publications on behalf of the European Geosciences Union.

Abstract

The Campbell–Stokes sunshine recorder (CSSR) has been one of the most commonly used instruments for measuring sunshine duration (SD) through the burn length of a given CSSR card. Many authors have used SD to obtain information about cloudiness and solar radiation (by using Ångström–Prescott type formulas). Contrarily, the burn width has not been used systematically. In principle, the burn width increases for increasing direct beam irradiance. The aim of this research is to show the relationship between burn width and direct solar irradiance (DSI), and to prove whether this relationship depends on the type of CSSR and burning card. A semi-automatic method based on image processing of digital scanned images of burnt cards is presented. With this method, the temporal evolution of the burn width with 1 min resolution can be obtained. From this, SD is easily calculated and compared with the traditional (i.e. visual) determination. The method tends to slightly overestimate SD but the thresholds that are used in the image processing could be adjusted to obtain an unbiased estimation. Regarding the burn width, results show that there is a high correlation between two different models of CSSRs, as well as a strong relationship between burn widths and DSI at a high-temporal resolution. Thus, for example, hourly DSI may be estimated from the burn width with higher accuracy than based on burn length (for one of the CSSR, relative root mean squared error 24 and 30 % respectively; mean bias error −0.6 and $-30.0\,W\,m^{-2}$ respectively). The method offers a practical way to exploit long-term sets of CSSR cards to create long time series of DSI. Since DSI is affected by atmospheric aerosol content, CSSR records may also become a proxy measurement for turbidity and atmospheric aerosol loading.

1 Introduction

Sunshine duration (SD) is a useful indicator of the amount of solar radiation arriving on the earth and a key variable for various sectors, including tourism, public health,

AMTD
7, 9537–9571, 2014

agriculture, and energy. According to the World Meteorological Organization (WMO, 2008), the SD for a given period is defined as the total time length of those sub-periods for which the direct solar irradiance exceeds 120 $W\,m^{-2}$. For climatological purposes, the units used are "hours per day", as well as percentage quantities, such as "relative daily sunshine duration" where SD is divided by the maximum possible SD (i.e., as if sky was clear all the time so a bright sun was present during the whole day, from sunrise to sunset).

One of the most used instruments to measure SD is the Campbell–Stokes sunshine recorder (CSSR). It was invented in the late 19th century to provide a measurement of the duration of bright sunlight by making a burn mark on a piece of specially treated cardboard. The measurement of the length of the burn for a given card gives daily SD. For details on the history of the CSSR, we refer to Stanhill (2003) and Sanchez-Lorenzo et al. (2013). In brief, the main parts of a current CSSR involve a sphere made of transparent glass, and a rounded metal plate placed behind the sphere. The glass sphere is designed to focus the Sun's rays onto a piece of recording cardboard. The metallic spherical part has three overlapping sets of grooves to hold the recording cards for the winter, summer and spring/autumn periods. The recording card has to be replaced daily after sunset. Hourly and half-hourly divisions are marked across the cards, enabling determination of the times of sunshine, with an estimated resolution of 0.1 h. For further details on the instrument and instructions for obtaining uniform results, as well as other traditional instruments for measuring SD, see Middleton (1969) and WMO (2008).

During the last few years, various automated instruments and other methods for obtaining SD have been developed, which are summarized in WMO (2008). One of these methods is the pyrheliometric method, which is based on direct irradiance measurements (e.g., Hinssen, 2006; Hinssen and Knap, 2007; Vuerich et al., 2012). Another way of determining SD is by means of automatic instruments specifically designed to this end, which have become commercially available (Wood et al., 2003; Kerr and Tabony, 2004; Matuszko, 2014). These instruments detect direct solar radiation and

AMTD
7, 9537–9571, 2014

count the time interval in which the irradiance exceeds a certain threshold. Progressively, many weather stations have changed traditional manual instruments (such as CSSR and Jordan photographic recorders) to these automatic systems. Moreover, different methods exist nowadays to estimate SD from geostationary satellite data, which potentially provide improved spatial coverage and representativeness (Olseth and Skartveit, 2001; Good, 2010; Kothe et al., 2013).

Despite the new models of sunshine recorders do not require daily attention by an observer and their data reduction (i.e., the process of filling and storing the SD data) is faster and more accurate, there is a consensus with regard to preserving CSSR type instruments at long-established (in some case, more than 120 years ago), well-maintained and freely exposed meteorological stations (Stanhill, 2003; Wood and Harrison, 2011; Sanchez-Lorenzo et al., 2013).

A change of the instrument used to measure SD can affect the homogeneity of the data series. This may lead to significant errors when evaluating trends and may hinder the possibility of determining long-term secular trends (Powell, 1983; Steurer and Karl, 1991; Brázdil et al., 1994; Stanhill and Cohen, 2008). Among the studies that analyze long series of SD, some works choose to restrict the period in order to avoid instrumental changes, therefore not encompassing the entire period of observation (Angell et al., 1984). Other studies assess the homogeneity of the SD series, such as research conducted in the United States (Cerveny and Balling, 1990; Stanhill and Cohen, 2005), UK (Kerr and Tabony, 2004), Iberian Peninsula (Guijarro, 2007; Sanchez-Lorenzo et al., 2007), Japan (Katsuyama, 1987; Stanhill and Cohen, 2008), China (Xia, 2010), and Switzerland (Sanchez-Lorenzo and Wild, 2012). The results of these studies point towards the need for further research including homogenization of the long-term SD series and the necessity of simultaneous measurements by both traditional and automatic instrumentation (Aguilar et al., 2003).

Differences between one type and another of SD measurements might be attributed to their particular characteristics and limitations. As the longer SD series are generally measured by using CSSR, the errors connected with this instrument are well-described

AMTD
7, 9537–9571, 2014

(Painter, 1981; Brázdil et al., 1994). Concretely, the two major problems with CSSR when comparing their measurements with other methods or instruments lie in the variability of the level of direct irradiance which produces a burn, and the overburning of the card in conditions of intermittent high irradiance (Stanhill, 2003). These difficulties can be added to the obvious element of subjectivity in measuring the burn length on the sunshine cards (Brázdil et al., 1994). The problem of overburning is very difficult to evaluate as one small burst of high direct irradiance causes a burn lasting far longer than the few seconds of its actual duration, and standard methods have therefore been proposed to take into account this fact when evaluating the burn lengths (WMO, 2008). Despite these rules, during events of very broken cloudiness, a measurement of SD by means of CSSR can be significantly overestimated (Painter, 1981; Kerr and Tabony, 2004).

Regarding the first problem, defining the direct irradiance value that produces burning ("burning threshold") is a well-known issue. One proof is the variability of values that the WMO has given: in 1971, WMO suggested that the threshold can vary between 70 and 280 $W\,m^{-2}$; in 1976, WMO recommended a threshold value of 200 $W\,m^{-2}$; finally, in 1981, a value of 120 $W\,m^{-2}$ was recommended (WMO, 2008). Gueymard (1993) tried to give some scientific justification to this value. Nevertheless, Bider (1958), Jaenicke and Kasten (1978) and Roldán et al. (2005) showed a large variety of burning thresholds for different CSSR. Similarly, Helmes and Jaenicke (1984) described the effects of using different types of recording cards. In addition, the measurement of threshold values indicated that there were notable losses of record which must be attributed to dew or other water deposits on the glass sphere. Painter (1981) obtained monthly averaged threshold values ranging from 16 to 142 $W\,m^{-2}$, despite some thresholds up to 400 $W\,m^{-2}$ were obtained in particular conditions. From the above discussion it is clear that long time series of SD include errors of several kinds and that their removal is a complicated problem. It is also important to stress that the problem of thresholds is not exclusive of CSSR, as it has been studied for other instruments such as the Foster sunshine recorder (Baker and Haines, 1969; Benson et al., 1984; Michalsky, 1992).

AMTD
7, 9537–9571, 2014

SD series also provide additional embedded information on other magnitudes. For example, many authors relate SD for a period of time with direct and global (which is the sum of the solar direct and diffuse contributions) irradiance, with the use of the so-called Ångström-Prescott type formulas (e.g., Sears et al., 1981; Benson et al., 1984; Martínez-Lozano et al., 1984; Stanhill, 1998; Power, 2001; Suehrcke, 2000; Bakirci, 2009), which were first proposed by Ångström (1924) and further modified by Prescott (1940). In addition, R. Jaenicke and L. Helmes developed a series of pioneering studies presenting a method to determine atmospheric turbidity from SD records (Jaenicke and Kasten, 1978; Helmes and Jaenicke, 1984, 1985, 1986), that has recently aroused interest (for a review, see Sanchez-Romero et al., 2014). SD data are also used in other fields such agriculture (Monteith, 1977; Stanhill and Cohen, 2001) or hydrological modeling (Döll et al., 2003).

This paper describes a new method to derive direct solar irradiance from the CSSR burnt cards by using digital image processing. The idea we assume here was first proposed by Wright (1935): the size of the burn at any point is related to the strength of the direct solar irradiance (DSI) focused on the card at that time. This hypothesis has recently been revisited, and several studies have shown the potential of the burn width of CSSR cards as a proxy for DSI (e.g., Wood and Harrison, 2011; Horseman et al., 2013), but here a more complete research is presented, comparing burn width and DSI for a relatively long period of time (2 years) and investigating results at higher temporal resolution (1 h). Section 2 provides a description of data and instruments used in this research. In Sect. 3, we describe the semi-automatic method proposed for determining the width of the burnt traces. In Sect. 4, we show the application of the new treatment of the CSSR cards to, first, determine the daily SD, and second, estimate the DSI at hourly resolution. Finally, conclusions of this study and suggestions for further research are presented in Sect. 5.

AMTD
7, 9537–9571, 2014

2 Instruments and data

Burnt cards from CSSRs and meteorological and radiative measurements used in the present study come from a weather and radiometric station located on the roof of a building of the University of Girona (41.962° N, 2.829° E, 115 m a.s.l.). Girona is a city located in the North-East of the Iberian Peninsula, at about 30 km from the Mediterranean Sea. The mean height of the horizon for the CSSRs is 4.2°, with a minimum of 0.2° at azimuth angle 86° W, and a maximum of 9.2° at azimuth angle 21° E (Fig. 1). Note that the Sun rises over the horizon at angular heights greater than 5°, while in the evening the Sun sets at much lower angular heights during most months. This means that the sunshine duration records and pyrheliometer measurements are slightly affected in the morning, but this issue does not affect the present research.

Two different models of CSSR have been used (Fig. 2a), with three different cards for each CSSR (Fig. 2b), which are used for different periods along the year. Hours and half-hours are printed in every card, as also shown in Fig. 2b. One of the CSSR and cards are from Thies Clima (hereafter referred to as CSSR1); the other CSSR is from Negretti and Zambra with cards of the model Mod.98 (hereafter referred to as CSSR2), formerly used by the Spanish Meteorological Agency (AEMET). DSI is measured by a pyrheliometer (CH-1 model) from Kipp and Zonen, mounted on a Sun tracker. The DSI is measured every second, and values are stored as 1 min averages. The station is also equipped with meteorological sensors to measure temperature, humidity, wind speed, precipitation, etc., as well as a ceilometer, a multifilter rotating shadowband radiometer and other radiometric sensors. In addition, a whole sky camera is continuously taken pictures of the sky dome.

We have processed 239 cards covering the period from January 2012 to January 2014 (2 years), for each type of CSSR. We have 94 winter cards (from 16 October to 28/29 February), 56 equinoctial cards (from 1 March to 15 April and from 1 September to 15 October) and 89 summer cards (from 16 April to 31 August).

AMTD
7, 9537–9571, 2014

3 Semi-automatic method for reading the burnt traces

We have developed a semi-automatic method to retrieve information from the burnt cards. We have considered "burnt" not only the perforated part, but also the black-grey area (scorched area) present on the edges of the burn. The method can be summarized in four steps. First, we scan each card on a suitable background. Second, we apply a digital process that increases the contrast of the burnt area. Thirdly, the center of the day (12 TST) on the card is determined. Finally, the burn width is measured, with the help of a computer program, along cross-sections spaced every minute. A schematic illustration of the different steps can be seen in Fig. 3. With this, we obtain daily evolution of the burn width on a resolution of 1 min; the length of the burn (i.e. sunshine duration) can be easily determined too. These four steps are detailed in the following sections. Our method presents similarities with the method by Horseman et al. (2013), but there are also significant differences, which will be highlighted below.

3.1 Image capture

Scanning the burnt card is the first step of our method. For this purpose, we use a commercial scanner (model HP Scanjet 5590). As sensors in image scanners alter with time and use, a method to calibrate the scanner must be applied regularly Horseman et al., 2013). On the other hand, we use a standard image format, 24-bit RGB BMP (bitmap), and the same dimension (2340 × 1700 pixels) for all scans. For scanning the cards, we use a green background (Fig. 3a) in order to obtain a contrast with the card, which is blue (face) and white (hour markers and other information). We use this contrast between the background and the card in the next steps to identify the burn and to establish the geometry of the card. The positioning of the card on the scanner does not need to be precise, which simplifies and speeds up the card scanning process. Before the scanning, an evaluation has been done to remove those cards that do not present any burn or to control those that present any anomalies (stains on the card face, deformations due to the rain, etc.).

AMTD
7, 9537–9571, 2014

3.2 Image treatment

On used cards, the edges of the burnt or scorched traces are, for the most part, black-brown, occasionally with some grey ash. As stated by Fan and Zhang (2013), there are not abrupt changes in grey intensity between the weak scorch and the card face, but their signatures on the RGB color coordinates are noticeably different. This fact will be the basis to identify the burnt parts of the card, by using the RGB image and the Image Processing Toolbox from MatLab. First, the white pixels in the image (so the markers of hours and half-hours, which are the only pixels reaching a high value in the red component) are identified by selecting the pixels with a high red component (we put a threshold of $R > 200$). With this, an image with "1" for white pixels and "0" for the rest of pixels is obtained; this image is called Im1. Secondly, we distinguish the pixels where the difference between red and blue components is less than 20 ($B-R < 20$), i.e., the green (background), black, grey, and white pixels. With this, an image is obtained where the pixels in blue areas are labeled as "0" and all the other pixels are labeled as "1"; this is image Im2. Then, we subtract Im1 from Im2 and set to 0 all pixels where the difference is negative. With this, an image of pixels labeled "1" for the burn and the background, and pixels labeled "0" for the non-burnt part of the card is obtained. There is still some "noise" in this image (that is, pixels of one kind surrounded by eight pixels of the other kind); this noise is removed from the image to obtain the final processed image (Fig. 3b, 1-pixels in white, 0-pixels in black). Note that all this process is automatic. The choice of the thresholds ($R > 200$ for Im1 and $B-R < 20$ for Im2) has been empirically determined after performing various checks and will certainly affect the identification of the burn but, as long as they are used consistently throughout the two card archives, their exact absolute values are not very important.

3.3 Image positioning

The positioning of the card within the image requires manual intervention, but it is necessary, not only for controlling the process, but also to be able to convert the image

AMTD
7, 9537–9571, 2014

of the burnt pixels into length (millimeters of width) and into time (minutes along the day). Depending on the shape of the card, we need to manually identify two or three points to find the center of the day (12 TST). More specifically, in curved cards (summer and winter cards) we mark three points (two on the ends of the outer arc and the third close to the center of the outer arc) to find the center and the radius of the outer circumferences (the same process could be applied for the inner arc). Then, as these cards are symmetric, it is easy to find all points in the image belonging to the outer or inner arc and the point corresponding to noon (Fig. 3c). In the equinoctial cards, the problem of finding the midday point is even easier than in the previous ones: knowing two points (at both ends of the outer – or inner – contour) provides sufficient information to locate the midday point.

From the image obtained in the previous step, the two points at the ends of the arcs could be found automatically reading across each row of the image starting from the left-hand edge and searching for a transition from the white to the black pixels (Horseman et al., 2013), but the geometry of Thies Clima cards is not simple enough. In addition, introducing a user intervention at this step (after applying the digital process) allows making a visual check to confirm that both the scan and treatment are correct before defining the midday point and continuing with the method.

3.4 Measurement of burning width

Unlike Horseman et al. (2013) method, in which the image of each card is rectified (that is, transformed to a representation with a straight burnt trace) before extracting the burn width, thus simplifying geometrical calculations, we consider here continuous radial sections that cover the whole card and measure the burn width (i.e., the length from the first to the last "burnt" pixels) along each section. As the size and shape of each card type is known and standardized, we know the radii of the outer and inner boundaries and their distance, so there is no need to cross the whole image, but only the area where the card is placed. For the equinoctial cards, parallel sections are performed instead of radial sections.

AMTD
7, 9537–9571, 2014

We continue by defining the relation between angular (or linear) displacement and time: as we know the angle (or distance) between the two edges that we defined in the previous step and we also know the period of time that correspond to these two points (this time is fixed in each type of card), the relation between angle (or distance) and time is immediate. So, if we want a 1 min resolution, we know to what angular (or linear) displacement corresponds. For example, for winter and summer cards, a 1 min displacement corresponds to an angular displacement of 0.064°; in the case of equinoctial cards, 1 min displacement corresponds to a linear displacement of 0.294 mm (0.317 mm) for CSSR1 (CSSR2). If we consider a resolution of one pixel, the resolution of the burn width is 0.126 mm in all cards.

As we know the point corresponding with 12 TST, consecutive angular displacements (corresponding to a 1 min temporal resolution) towards the left are applied, the radial sections between the inner radius to the outer radius are inspected, and the distance between the first "1" pixel to the last "1" pixel in the radial section is computed. Thus, we obtain the temporal evolution of the burn width for the morning. We do in a similar way (but towards the right) to obtain the afternoon evolution of the burn width. With this, the daily evolution of the burn width in each card is finally obtained (Fig. 3d). Note that all processes in this step are fully automatic.

4 Applications of the measurements of the burn width

The semi-automatic method proposed to process the burnt cards is useful for the characterization of the CSSRs. This can help in the assessment of different types of errors that can affect the SD measurements, which can result in the inhomogeneity of a long-term series of SD (Sect. 4.1). Moreover, the method can also be useful in order to provide a record of DSI, since the burn width can be used as a proxy for pyrheliometer measurements (Sect. 4.2).

AMTD
7, 9537–9571, 2014

4.1 Assessment of the measurement of sunshine duration

As summarized by Brázdil et al. (1994), the sources of errors in the SD series provided by the CSSRs are (i) the ageing of the glass ball, which with increasing operation time becomes less efficient, (ii) the replacement of the recorder by a new device manufactured by different companies, and (iii) the variability of the recording card (e.g. different quality, color, or material). In order to homogenize the worldwide measurements of SD, a specific design of the CSSR was recommended as the reference in the 1960s (WMO, 1962). This, however, did not overcome all the problems, especially when long-term series with records before and after 1960s are used to study SD trends. So, here we will quantify these errors/differences in the observations by using our digital method applied to two different CSSRs that use different burning cards.

One of the major problems when comparing SD measurements from different CSSR devices and card types is the variability of the level of DSI that produces a burn (e.g., Stanhill, 2003; Sanchez-Romero et al., 2014). If we consider the threshold of 120 $W\,m^{-2}$ in DSI in order to calculate SD (SDpyr method) the mean value found for our database is 7.16 h, which can be taken as the reference (correct value) for other estimations. Table 1 shows the mean value obtained when using different methods of estimating SD applied both to CSSR1 and CSSR2. To obtain SD with the above described semi-automatic method (SDaut), all minutes showing burning are accounted. As shown in Fig. 4a for CSSR1, retrieved SD using the SDaut and the SDpyr methods agree very well (correlation coefficients higher than 0.98 for both instruments), although a minor overestimation is apparent. Semi-automatic method gives a mean SD deviation with respect SDpyr of 0.37 h (4.9 %) and 0.06 h (0.8 %) for CSSR1 and CSSR2 respectively. Then both instruments give a slight overestimation of SD, more pronounced for CSSR1, which shows a somewhat higher sensitivity than CSSR2. The instrument sensitivities can be also quantified searching for the DSI threshold values that would give the corresponding mean SDaut: 55 and 110 $W\,m^{-2}$ respectively for CSSR1 and CSRR2.

AMTD
7, 9537–9571, 2014

The latter threshold values, found to agree with SDaut method, are lower than the 120 W m^{-2} suggested by the WMO. This results from the overestimation in SD given by SDaut, which was expected because some instructions and recommendations (WMO, 2008) are not applied in the method. For example, when SD is retrieved by reading the cards manually (SDman method), in the case of a clear burn with round ends, the time length is reduced at each end by an amount equal to half the radius of curvature of the end of the burn; or, in the case of a clear burn that is temporarily reduced in width by at least one third, an amount of 0.1 h is subtracted from the total length of the burnt segment. Contrarily, SDaut accounts strictly for all minutes where a burn (or a scorch) is detected, without any further correction, so it tends to – slightly – overestimate SD. Among the possible improvements in the SDaut method, the introduction of the advices proposed by WMO (WMO, 2008) in the algorithm would reduce the differences between SDaut and SDpyr.

Table 1 also shows the mean SD that is obtained by SDman method (we processed all cards in the usual, visual way): as expected they are slightly lower than values found with SDaut method, but the general agreement between SDaut and SDman methods is very good for both instruments: the mean deviation of SDaut with respect SDman is 0.22 h (2.9 %) for CSSR1 and only 0.12 h (1.7 %) for CSSR2. Figure 4a shows (for CSSR1) the excellent agreement between daily SD obtained from both SDaut and SDman methods with SDpyr. It is important to notice that, for low values of SD, SDman gives also higher values than SDpyr (as it does SDaut): this must be related to the overburning of the card in conditions of broken cloudiness (Stanhill, 2003; Sanchez-Romero et al., 2014).

From the above results, we confirm that 120 W m^{-2} is a suitable DSI threshold. Nevertheless, it is worth noting that there is a high variability in the exact threshold that gives the best agreement of SD for each particular card along the year (not shown). This large seasonal variability was pointed out by Painter (1981), Michalsky (1992) or Roldán et al. (2005). The position of the card on the CSSR, the humidity conditions (Bider, 1958; Painter, 1981), and the poor horizon at the location of the instruments

AMTD
7, 9537–9571, 2014

(especially in the morning between October and April) are factors that could explain such high variability.

The differences between instruments are evident in Fig. 4b and in Table 1. CSSR1 gives slightly lower values than CSSR2 for both SDaut and SDman methods. It can be due to the ageing of the glass sphere as the latter is an instrument from the 1980s and the former was brand new at the beginning of our research, although it could also be related to the different quality and colors of the recording cards used for each device (Brázdil et al., 1994). In this sense, note that the semi-automatic method uses the same threshold values in the image segmentation when defining the burnt regions for both types of CSSR and cards; an improved method could tune a particular color threshold for each CSSR or card in order for SDaut to match almost exactly SDpyr (or SDman if pyrheliometric measurements are not available).

All mean differences found are similar to the uncertainty usually assigned to the measurement of SD (i.e., 0.1 h), and even in the case of the automatic method, the difference between both CSSR is much lower than the maximum errors of around 7 % suggested by Brázdil et al. (1994) referring to different instruments or to the ageing of the glass sphere. In fact, other radiometric variables have similar or even higher uncertainties: global solar radiation has instrumental errors of around 5 % and 2 % for the monthly and annual means, respectively (Gilgen et al., 1998; for more information about instrumental errors of radiation data, see for example Vignola et al., 2012). With the improvements proposed above, not only the linear-relationship between SDman and SDaut would be even better, but also the differences between two different CSSR would be reduced to become almost null.

4.2 Burn width and its relationship with direct solar irradiance

Figure 5a and b shows the daily evolution of the burn width for the two CSSR and for two different days (one mostly sunny and the other with scattered and broken cloudiness). In this figure, and hereafter, we refer to the burn width for CSSR1 and CSSR2 as h1 and h2 respectively. It is evident that the evolution of the burn width shows an

AMTD
7, 9537–9571, 2014

excellent agreement for both recorders (and also with DSI), with a correlation coefficient higher than 0.90 when all the 1 min records are taken. Nevertheless, for some days, there might be a lag of up to a few minutes between CSSR and DSI data. This is likely the result of a slight misalignment of the cards from their correct position in the CSSR device. Thus, if analysis with less than a few minutes resolution is to be performed, we would need to consider this misalignment; in the present study, hourly averages of burn width and of DSI will be used onwards. As an example of the strong relationship, Fig. 5c shows the scatterplot, the linear fit, and the correlation coefficient of h2 against h1 on hourly basis. Note that the slope of the linear regression is lower than 1, i.e. burn width on CSSR1 is notably higher than that on CSSR2, as was expected given the higher sensitivity of CSSR1 found above. The same analyses have been performed separately for each set of seasonal cards (not shown) and it turns out that the correlation coefficients are almost 1 for all card types and the slopes of the linear regressions are also very similar for all seasons. In other words, the relationship between h1 and h2 is almost constant during the year.

The mean difference between h1 and h2 is 1.03 mm at 1 min resolution, which is a relative difference of 32 % respect h1 (much higher than the difference in daily SD). This value agrees with the slope of the fit of hourly averages (0.69) which points to a relative difference of 31 %. Wood and Harrison (2011) already stated that the burns in one site could be thinner than those in another site although DSI conditions were the same (due to differences among instruments), as we find in our study. So, even though h1 and h2 are highly correlated with each other, it will be important to know which instrument has been used if the burn width data is to be used, by fitting some convenient parameters, to estimate other magnitudes such as DSI. This is similar to what happens with Angstrom–Prescott equations that relate global solar radiation with SD, where their parameters depend on local calibration (Martínez-Lozano et al., 1984). Note, however, that the latter parameters must be adjusted basically because of different climates (typical atmospheric turbidity) while the former depend basically on the specific instrument.

AMTD
7, 9537–9571, 2014

In Fig. 5a and b we can also see the daily evolution of DSI. The evolution of DSI and that of h1 and h2 shows a strong relationship, which is also displayed in Fig. 6, that suggest us to propose a certain fit between burn width and DSI. Wright (1935) and Lally (2008) proposed an exponential fit for the estimation of DSI from burn width. These studies did not consider too many days and probably that is the reason why they did not find that increasing burn width tends to a certain maximum value of DSI, as a horizontal asymptote. This is seen in Fig. 6: from a certain value of burn width, the value of DSI does not vary too much and tends to a maximum value. So, in order to do a fit considering an exponential growing and a horizontal asymptote, a logistic function is proposed:

$$\mathrm{DSI} = \frac{L}{1 + K e^{-G h'}} \quad (1)$$

In this equation, h' is the normalized burn width (i.e. the value of burn width divided by its 95-percentile value, for each CSSR). The function depends on some parameters having physical meanings: L is fixed to the 95-percentile value of DSI, K is related to the threshold DSI (i.e. the DSI value in the y intercept), and G is related to the growth ratio. We consider K and G as the free-parameters for the fit. Figure 6 shows the scatterplot between burn width and DSI, the logistic fit, and the correlation coefficient for the two CSSRs, on hourly basis. We can see that the growth ratio (G value) is similar in both CSSRs and that the K value is higher in CSSR1 than CSSR2, which agrees with the fact that CSSR1 has a lower DSI threshold than CSSR2 because CSSR1 is more sensitive than CSSR2.

We compare our method based on measuring the burn width with the estimations of DSI using hourly SD (i.e., counting the minutes with burn within each hour). Stanhill (1998) presented a similar approach, and suggested both linear and quadratic regressions, but for our data we have found more appropriate to fit exponential functions, which are shown in Fig. 7 for both CSSRs. It is important to note that values of DSI for SD equal to 1 h (that is, for sun shining along the whole hour) range from 200 to

AMTD
7, 9537–9571, 2014

1000 W m^{-2}, thus making it difficult to obtain a good estimation of DSI for completely clear-sky hours. In addition, the cases of SD equal to 1 h are the most probable (more than 62 % of all the cases for the two CSSRs).

As seen in Fig. 5a and b, DSI affects burn width at very short time scales (1 min), but the advantages of using the burn width instead of SD to estimate DSI even at hourly resolution are proven in Table 2 and in Fig. 8. In Table 2 we can see, for each method, different statistical indexes comparing the estimated DSI with the measured DSI, along with the parameters describing the relationship between both variables (all indexes and parameters are defined in Table 2). It is clear that the method based on burn width gives better results, especially if we look the column of MBE and the *B* value (intercept), and also regarding the relative root mean squared error RRMSE. These results show that the burn width gives more information of the variation of DSI on high-resolution temporal data (1 h) whereas counting the time length of the burn for short periods only gives information whether the sun is visible (i.e., whether DSI is higher than a certain value). It is remarkable that the correlation between DSI and burn width at hourly resolution is as good as other relationships found by other authors at lower temporal resolution (daily, monthly, seasonally or annually) using only SD and linear and quadratic correlations (Benson et al., 1984; Louche et al., 1991; Nfaoui and Buret, 1993; Maduekwe and Chendo, 1995; Stanhill, 1998; Power, 2001).

In Fig. 8, box plots for the residuals between the estimated and measured DSI, in bins of 100 W m^{-2} width, are represented for the two methods: (a) estimation of DSI based on burn width and (b) estimation of DSI based on SD (only results for CSSR1 are presented, as they are similar for CSSR2). Again, the burn width method gives better mean values and less dispersion than the SD method. Note that the burn width method can give values of DSI up to 925 W m^{-2} (the parameter *L* in the method) covering nearly the whole DSI range, while SD method can not give values above 673 W m^2 (for CSSR1, and according to the exponential fit found for our data). This is a consequence of what it was said before: for hourly SD close to 1 h it is not possible to distinguish values of DSI ranging from 200 to 1000 W m^{-2}.

AMTD
7, 9537–9571, 2014

5 Conclusions and future research

In this study we propose a new semiautomatic method to obtain the temporal evolution of the burn width in Campbell–Stokes sunshine recorder (CSSR) cards. This method is also capable to produce very good results as far as sunshine duration (SD) measurements are concerned. The mean overestimation in daily SD derived from this method, when compared with the value from a pyrheliometer by using the standard threshold in DSI of 120 $W m^{-2}$, are less than 5 %, which is very close to the accepted uncertainty of the traditional manual screening of cards. Differences could be reduced if several advices proposed by WMO were taken into account regarding the rounded ends of the burnt areas, and the cases of intermittent burning. In addition, the thresholds applied in the image processing could be defined differently for each card type. These improvements, however, will be the subject of future research.

The two CSSRs studied here give almost the same SD, despite of different geometries and cardboard types, but one recorder (CSSR1) is slightly more sensitive than the other, therefore producing systematically longer SD. The difference, however, is very small (mean bias of 0.1–0.3 h depending on the method – manual or automatic) and of the same order of the instrumental uncertainty. Note that the threshold values that should be applied to DSI for an exact match of CSSR SD values should be 55 and 110 $W m^{-2}$ respectively, which reflect again the slightly different sensitivity. Nevertheless, the different sensitivity of the instruments is reflected in the burn width measurements: the mean relative difference is about 30 % (CSSR1 burns wider than CSSR2 burns). So, it is important to know which instrument has been used if we want to estimate other magnitudes such as DSI.

Hourly DSI can be satisfactorily estimated from the burn width measurements. The estimation based on burn width by using a logistic fit is better than that based on counting the time length of the burn (i.e. hourly SD). For example, in the case of CSSR1, we have obtained a MBE of $-0.6 W m^{-2}$, a coefficient of determination of 0.81 and a relative root mean squared error of 24 %, when comparing hourly DSI estimations

AMTD
7, 9537–9571, 2014

from burn width with actual measurements (the corresponding values for CSSR2 are 6.6 W m^{-2}, 0.75, 27 %). These indexes are notably better than those obtained when SD is used (−30 W m^{-2}, 0.70, 30 % approximately for the two instruments). This result shows that the burn width gives more information of the variation of DSI on high-resolution temporal data, meanwhile the other method is useful only for estimations for longer periods (e.g. daily). As different CSSRs have different sensitive to DSI, the parameters of the equation that relates burn width with DSI have to be found for each case. Specifically, these parameters are related with the sensitivity of the instrument and the maximum DSI of the region.

Future research may consider taking into account not only the burn width, but also the perforated part of the burn (Roberts, 2012). It is not the same 2 mm of burn width without perforation that the same 2 mm but with 1 mm of perforation and 1 mm of scorch: a priori, more perforated part on the burn width would mean higher DSI. Moreover, further analysis needs to consider the temporal misalignment between the burn and DSI measurements if analyses with less than a few minutes resolution are to be performed.

Once this method is implemented, other magnitudes can be introduced. Since DSI is affected by atmospheric turbidity, especially at times near sunrise and sunset because of the longer optical path, having an estimation of DSI from the burn width may be used to estimate turbidity. Moreover, if cloud conditions are screened out, the presence or absence of burn at certain times may be an indicator of low or high aerosol load (and water vapor content) in the atmospheric column: in particular just after sunrise and before sunset, DSI may be unable to burn the CSSR card if it is much lower than it would be in a dry, clean atmosphere.

So, the measurements of burn width in CSSR cards obtained from the semi-automatic method described in this study can provide a way to create time series of solar irradiance in less than daily resolution. We have shown that it is possible to use readily available technology to mine the archives of a simple, reliable and widely used meteorological instrument to provide a proxy record of DSI. In fact, the reconstruction

AMTD
7, 9537–9571, 2014

can reach as much as around 120 years from the present day as long-term records of SD cards are available at some historical meteorological stations such as, for example, the Blue Hill Observatory in Milton, Massachusetts (US), where CSSR cards have been stored since the late-1880s (Magee et al., 2014; M. Iacono, personal communication, 2014).

Acknowledgements. This research was supported by the Spanish Ministry of Science and Innovation project NUCLIERSOL (CGL2010-18546). The first author enjoys a grant by the FPU program (FPU AP2010-0917) of the Spanish Ministry of Education. ASL was supported by a postdoctoral fellowship from the "Secretaria per a Universitats i Recerca del Departament d'Economia i Coneixement, de la Generalitat de Catalunya i del programa Cofund de les Accions Marie Curie del 7è Programa marc d'R+D de la Unió Europea" (2011 BP-B 00078).

References

Aguilar, E., Auer, I., Brunet, M., Peterson, T. C., and Wieringa, J.: Guidelines on Climate Metadata and Homogenization, Malaga, 2003.

Angell, J. K., Korshover, J., and Cotton, G. F.: Variation in United States cloudiness and sunshine, 1950–82, J. Clim. Appl. Meteorol., 23, 752–760, 1984.

Ångström, A.: Solar and terrestrial radiation, Q. J. Roy. Meteor. Soc., 50, 121–125, 1924.

Baker, D. G. and Haines, D. A.: Solar Radiation and Sunshine Duration Relationships in the North-Central Region and Alaska, Agricultural Experiment Station, University of Minnesota, 1969.

Bakirci, K.: Correlations for estimation of daily global solar radiation with hours of bright sunshine in Turkey, Energy, 34, 485–501, doi:10.1016/j.energy.2009.02.005, 2009.

Benson, R. B. B., Paris, M. V. V, Sherry, J. E. E., and Justus, C. G. G.: Estimation of daily and monthly direct, diffuse and global solar radiation from sunshine duration measurements, Sol. Energy, 32, 523–535, doi:10.1016/0038-092X(84)90267-6, 1984.

Bider, M.: Uber die Genauigkeit der Registrierungen des Sonnenscheinautographen Campbell–Stokes, Arch. Meteor. Geophy. B., 9, 1922–230, 1958.

AMTD

7, 9537–9571, 2014

Brázdil, R., Flocas, A. A., and Sahsamanoglou, H. S.: Fluctuation of sunshine duration in central and south-eastern Europe, Int. J. Climatol., 14, 1017–1034, doi:10.1002/joc.3370140907, 1994.
Cerveny, R. and Balling, R. C.: Inhomogeneities in the long-term United States' sunshine record, J. Climate, 3, 1045–1048, 1990.
Döll, P., Kaspar, F., and Lehner, B.: A global hydrological model for deriving water availability indicators: model tuning and validation, J. Hydrol., 270, 105–134, doi:10.1016/S0022-1694(02)00283-4, 2003.
Fan, Q. and Zhang, Y.: A scorch extraction method for the Campbell–Stokes sunshine recorder based on multivariable thresholding, in: International Conference on Imaging Systems and Techniques, Beijing 2013.
Gilgen, H., Wild, M., and Ohmura, A.: Means and trends of shortwave irradiance at the surface estimated from global energy balance archive data, J. Climate, 11, 2042–2061, 1998.
Good, E.: Estimating daily sunshine duration over the UK from geostationary satellite data, Weather, 65, 324–328, 2010.
Gueymard, C.: Analysis of monthly average solar radiation and bright sunshine for different thresholds at Cape Canaveral, Florida, Sol. Energy, 51, 139–145, 1993.
Guijarro, J. A.: Cambios en la medida de las horas de insolación: análisis de su impacto en dos observatorios de las Islas Baleares (España), Rev. Climatol., 7, 27–32, 2007.
Helmes, L. and Jaenicke, R.: Experimental verification of the determination of atmospheric turbidity from sunshine recorders, J. Clim. Appl. Meteorol., 23, 1350–1353, 1984.
Helmes, L. and Jaenicke, R.: Hidden information within series of measurements – four examples from atmospheric sciences, J. Atmos. Chem., 3, 171–185, 1985.
Helmes, L. and Jaenicke, R.: Atmospheric turbidity determined from sunshine records, J. Aerosol Sci., 17, 261–263, 1986.
Hinssen, Y. B. L.: Comparison of Different Methods For the Determination of Sunshine Duration, De Bilt, 2006.
Hinssen, Y. B. L. and Knap, W. H.: Comparison of pyranometric and pyrheliometric methods for the determination of sunshine duration, J. Atmos. Ocean. Tech., 24, 835–846, doi:10.1175/JTECH2013.1, 2007.
Horseman, A. M., Richardson, T., Boardman, A. T., Tych, W., Timmis, R., and MacKenzie, A. R.: Calibrated digital images of Campbell–Stokes recorder card archives for direct solar irradiance studies, Atmos. Meas. Tech., 6, 1371–1379, doi:10.5194/amt-6-1371-2013, 2013.

AMTD
7, 9537–9571, 2014

Jaenicke, R. and Kasten, F.: Estimation of atmospheric turbidity from the burned traces of the Campbell–Stokes sunshine recorder, Appl. Optics, 17, 2617–2621, 1978.
Katsuyama, M,: On comparison between rotating mirror sunshine recorders and Jordan sunshine recorders, Weather Serv. Bull., 54, 169–183, 1987 (in Japanese).
Kerr, A. and Tabony, R.: Comparison of sunshine recorded by Campbell–Stokes and automatic sensors, Weather, 59, 90–95, doi:10.1256/wea.99.03, 2004.
Kothe, S., Good, E., Obregón, A., Ahrens, B., and Nitsche, H.: Satellite-based sunshine duration for Europe, Remote Sens., 5, 2943–2972, doi:10.3390/rs5062943, 2013.
Lally, M. J.: Solar beam intensity inferred from Campbell–Stokes Sunshine Records, University of Reading, UK, 24 pp., 2008.
Louche, A., Notton, G., Poggi, P., and Simonnot, G.: Correlations for direct normal and global horizontal irradiation on a French Mediterranean site, Sol. Energy, 46, 261–266, doi:10.1016/0038-092X(91)90072-5, 1991.
Maduekwe, A. A. L. and Chendo, M. A. C.: Predicting the components of the total hemispherical solar radiation from sunshine duration measurements in Lagos, Nigeria, Renew. Energ., 6, 807–812, 1995.
Magee, N. B., Melaas, E., Finocchio, P. M., Jardel, M., Noonan, A., and Iacono, M. J.: Blue Hill Observatory sunshine – assesment of climate signals in the longest continuous meteorological record in North America, B. Am. Meteorol. Soc., doi:10.1175/BAMS-D-12-00206.1, online first, 2014.
Martínez-Lozano, J. A., Tena, F., Onrubia, J. E., and De La Rubia, J.: The historical evolution of the Ångström formula and its modifications: review and bibliography, Agr. Forest Meteorol., 33, 109–128, 1984.
Matuszko, D.: A comparison of sunshine duration records from the Campbell–Stokes sunshine recorder and CSD3 sunshine duration sensor, Theor. Appl. Climatol., doi:10.1007/s00704-014-1125-z, online first, 2014.
Michalsky, J. J.: Comparison of a National Weather Service Foster Sunshine Recorder and the World Meteorological Organization Standard for sunshine duration, Sol. Energy, 48, 133–141, 1992.
Middleton, W. E. K.: Invention of the Meteorological Instruments, The Johns Hopkins University Press, 1969.
Monteith, J. L.: Climate and the efficiency of crop production in Britain, Philos. T. R. Soc. Lond., 281, 277–294, 1977.

AMTD
7, 9537–9571, 2014

Nfaoui, H. and Buret, J.: Estimation of daily and monthly direct, diffuse and global solar radiation in Rabat (Morocco), Renew. Energ., 3, 923–930, 1993.
Olseth, J. A. and Skartveit, A.: Solar irradiance, sunshine duration and daylight illuminance derived from METEOSAT data for some European sites, Theor. Appl. Climatol., 69, 239–252, 2001.
Painter, H. E.: The performance of a Campbell–Stokes sunshine recorder compared with a simultaneous record of a normal incidence irradiance, Meteorol. Mag., 110, 102–109, 1981.
Powell, G. L.: Instrumental effects on the sunshine record, J. Clim. Appl. Meteorol., 22, 962–963, 1983.
Power, H. C.: Estimating clear-sky beam irradiation from sunshine duration, Sol. Energy, 71, 217–224, 2001.
Prescott, J.: Evaporation from a water surface in relation to solar radiation, Trans. R. Soc. Sci. Aust., 64, 114–125, 1940.
Roberts, C. J.: Recovering Direct Solar Downwelling Flux Time Series from the Campbell–Stokes Sunshine Card Archive, University of Birmingham, 221 pp., 2012.
Roldán, A., Righini, R., and Grossi Gallegos, H.: Preliminary analysis of tghe Behaviour of the cards used in the Argentine sunshine recorders, Av. en Energías Renov. y Medio Ambient, 9, 9–13, 2005.
Sanchez-Lorenzo, A., Brunetti, M., Calbó, J., and Martin-Vide, J.: Recent spatial and temporal variability and trends of sunshine duration over the Iberian Peninsula from a homogenized data set, J. Geophys. Res., 112, D20115, doi:10.1029/2007JD008677, 2007.
Sanchez-Lorenzo, A., Calbó, J., Wild, M., Azorin-Molina, C., and Sanchez-Romero, A.: New insights into the history of the Campbell–Stokes sunshine recorder, Weather, 68, 326–327, doi:10.1002/wea.2156, 2013.
Sanchez-Lorenzo, A. and Wild, M.: Decadal variations in estimated surface solar radiation over Switzerland since the late 19th century, Atmos. Chem. Phys., 12, 8635–8644, doi:10.5194/acp-12-8635-2012, 2012.
Sanchez-Romero, A., Sanchez-Lorenzo, A., Calbó, J., González, J. A., and Azorin-Molina, C.: The signal of aerosol-induced changes in sunshine duration records: a review of the evidence, J. Geophys. Res.-Atmos., 119, 4657–4673, 2014.
Sears, R. D., Flocchini, R. G., and Hatfield, J. L.: Correlations of total, diffuse and direct solar radiation with the percentage of possible sunshine for Davis, California, Sol. Energy, 27, 357–360, doi:10.1016/0038-092X(81)90070-0, 1981.

AMTD
7, 9537–9571, 2014

Stanhill, G.: Estimation of direct solar beam irradiance from measurements of the duration of bright sunshine, Int. J. Climatol., 18, 347–354, doi:10.1002/(SICI)1097-0088(19980315)18:3<347:AID-JOC239>3.0.CO;2-O, 1998.
Stanhill, G.: Through a glass brightly: some new light on the Campbell–Stokes sunshine recorder, Weather, 58, 3–11, 2003.
Stanhill, G. and Cohen, S.: Global dimming: a review of the evidence for a widespread and significant reduction in global radiation with discussion of its probable causes and possible agricultural consequences, Agr. Forest Meteorol., 107, 255–278, doi:10.1016/S0168-1923(00)00241-0, 2001.
Stanhill, G. and Cohen, S.: Solar radiation changes in the United States during the Twentieth Century: evidence from sunshine duration measurements, J. Climate, 18, 1503–1512, 2005.
Stanhill, G. and Cohen, S.: Solar radiation changes in Japan during the 20th Century: evidence from sunshine duration measurements, J. Meteorol. Soc. Jpn., 86, 57–67, 2008.
Steurer, P. M. and Karl, T. R.: Historical sunshine and cloud data in the United States, Oak Ridge National Laboratory, Pennsylvania Stat University, United States, 1991.
Suehrcke, H.: On the relationship between duration of sunshine and solar radiation on the Earth's surface: Ångström's equation revisited, Sol. Energy, 68, 417–425, 2000.
Vignola, F., Michalsky, J., and Stoffel, T.: Solar and Infrared Radiation Measurements, CRC Press, Boca Raton, Florida, 2012.
Vuerich, E., Morel, J. P., Mevel, S., and Oliviéri, J.: Updating and development of methods for worldwide accurate measurements of sunshine duration, in: TECO – 2012, vol. 1984, Brussels, 2012.
WMO: Abridge Final Report of the Third Seasson of the Commission For Instruments and Methods of Observations, WMO-No. 116, Geneva, Switzerland, 1962.
WMO: Guide to Meteorological Instruments and Methods of Observation, 7th edn., Geneva, Switzerland, 2008.
Wood, J., Muneer, T., and Kubie, J.: Evaluation of a new photodiode sensor for measuring global and diffuse irradiance, and sunshine duration, J. Sol. Energ.-T. ASME, 125, 43, doi:10.1115/1.1531149, 2003.
Wood, R. C. and Harrison, R. G.: Scorch marks from the sky, Weather, 66, 39–41, doi:10.1002/wea.664, 2011.
Wright, H. L.: Some Notes on Readings at Kew Observatory of the Gorczynski Pyrheliometer the Sunshine Recorder and the Black Bulb Thermometer, London, 1935.

AMTD
7, 9537–9571, 2014

Xia, X.: Spatiotemporal changes in sunshine duration and cloud amount as well as their relationship in China during 1954–2005, J. Geophys. Res., 115, D00K06, doi:10.1029/2009JD012879, 2010.

AMTD
7, 9537–9571, 2014

Table 1. The first two columns are the mean value of SD by manual and semiautomatic methods, respectively. The third column is the value of SD from pyrheliometric method by using a DSI threshold (in parenthesis) that would approach the corresponding mean SD using the semiautomatic method. Recall that the "true" mean SD (by using 120 $W\,m^{-2}$ as the DSI threshold) is 7.16 h.

	Manual	Semiautomatic	DSI threshold
SD1	7.31 h	7.53 h	7.49 h (55 $W\,m^{-2}$)
SD2	7.10 h	7.22 h	7.21 h (110 $W\,m^{-2}$)

AMTD
7, 9537–9571, 2014

Table 2. Statistical parameters of estimations of hourly DSI when compared with DSI measurements, by different methods and instruments (from mean burn width, h1, h2; from hourly sunshine duration, SD1, SD2; from Stanhill (1998) study). MBE is the mean bias error; RMSE is the root mean square error; RRMSE is the relative root mean square error; R^2 is the coefficient of determination; A is the slope of the regression line; and B is the y intercept of the regression line.

Method	MBE ($W\,m^{-2}$)	RMSE ($W\,m^{-2}$)	RRMSE (%)	R^2	A	B ($W\,m^{-2}$)
h1	−0.6	129	23.9	0.81	1.00	−3.20
h2	6.6	147	27.1	0.75	1.01	−1.23
SD1	−30.0	165	30.5	0.70	0.98	−16.7
SD2	−29.0	159	29.0	0.71	0.98	−20.7
Stanhill (linear)	–	–	48.4	0.74	–	–
Stanhill (quadratic)	–	–	44.7	0.78	–	–

AMTD
7, 9537–9571, 2014

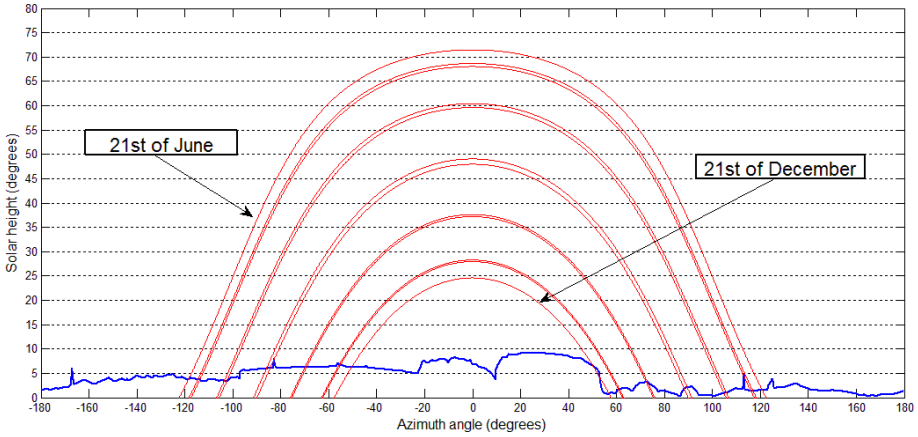

Figure 1. Solar path for the 21 each month (red lines) and horizon height for each azimuth angle (blue line).

AMTD
7, 9537–9571, 2014

Figure 2. (a) Details of the two different CSSRs mounted in Girona (NE Spain), and **(b)** an example of the 3 types of cards used during summer, winter and equinoctial seasons, respectively (the longer the daylight hours, the longer the card).

AMTD
7, 9537–9571, 2014

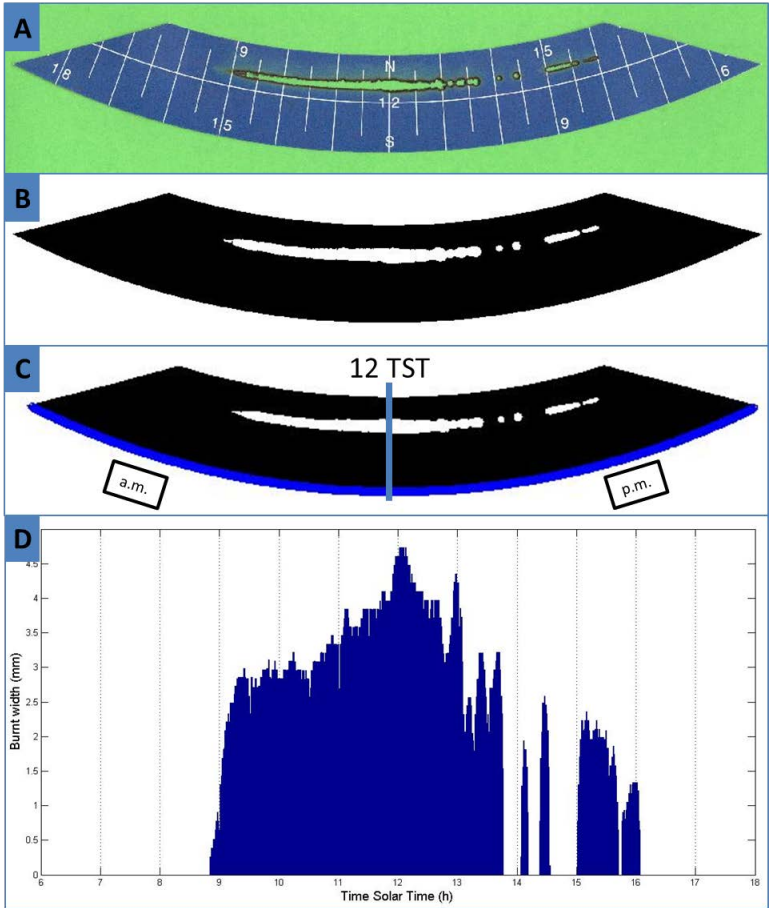

Figure 3. Steps of the semi-automatic method for retrieving information from the CSSR burned cards and for a certain day: **(a)** captured image, **(b)** treated image, **(c)** positioned image and **(d)** measured burn width along time.

AMTD
7, 9537–9571, 2014

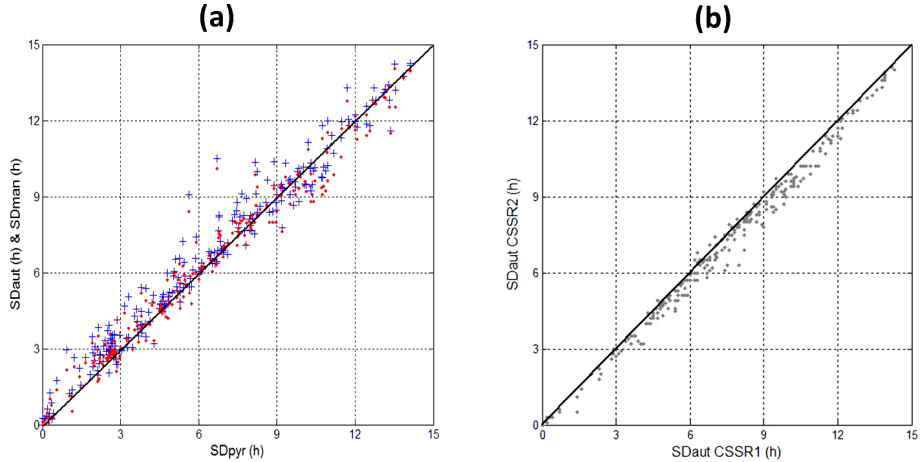

Figure 4. Scatterplots of the **(a)** daily SD obtained for CSSR1 from both SDaut (blue crosses) and SDman (red points) methods against SDpyr, considering the threshold of 120 $W\,m^{-2}$ in DSI; and **(b)** the daily SD obtained by the two CSSR using the automatic method. In each graphic we also represent the 1 : 1 line (black line).

AMTD
7, 9537–9571, 2014

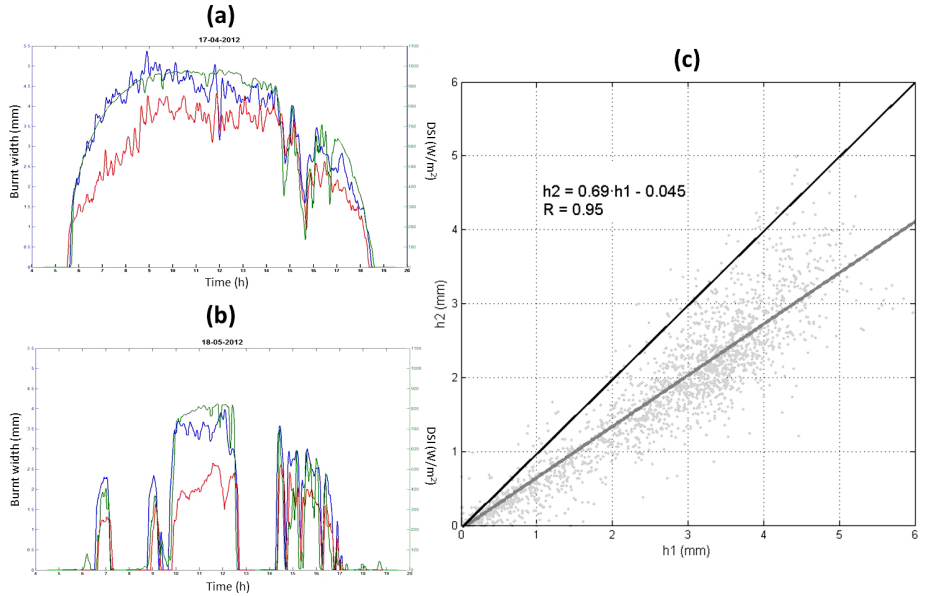

Figure 5. (a, b) Daily evolution of burn width (blue line for CSSR1 and red line for CSSR2) and DSI (green line) for two different days. **(c)** Scatterplot of the burn width in CSSR2 (h2) vs. that of CSSR1 (h1) on hourly resolution. We also represent the 1 : 1 line (black line) and the linear regression fit (green line).

AMTD
7, 9537–9571, 2014

Digital image processing of sunshine recorder cards

A. Sanchez-Romero et al.

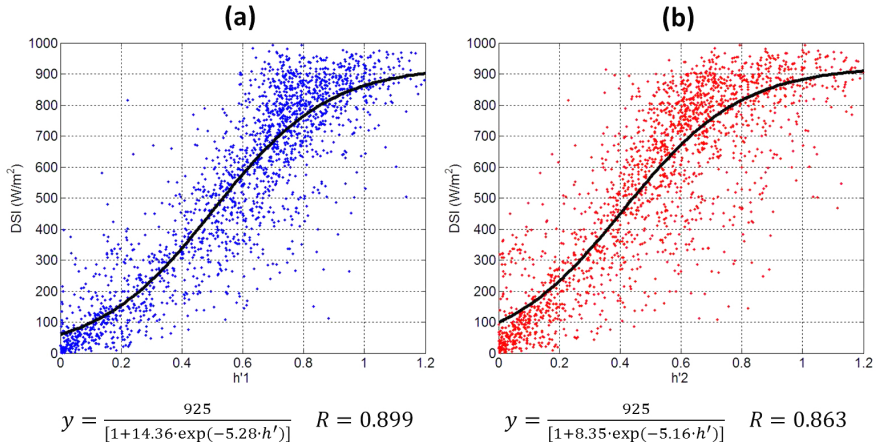

Figure 6. (a) Scatterplots of the DSI against normalized width for CSSR1, in hourly resolution. The fitted logistic function and the correlation coefficient are also shown (black line). **(b)** The same but for CSSR2.

AMTD
7, 9537–9571, 2014

Digital image processing of sunshine recorder cards

A. Sanchez-Romero et al.

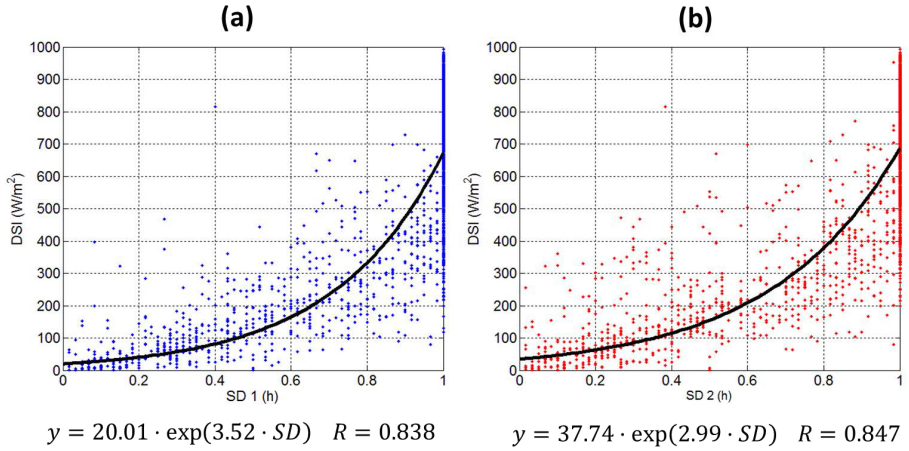

Figure 7. (a) Scatterplots of the DSI against SD for CSSR1 on hourly resolution. The exponential regression (black line) and the correlation coefficient are also displayed. **(b)** The same but for CSSR2.

AMTD
7, 9537–9571, 2014

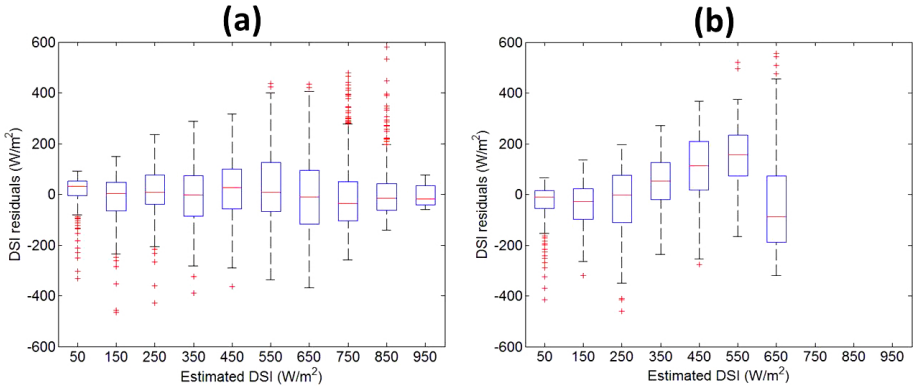

Figure 8. Box plots of the differences between estimated and true DSI for **(a)** estimation based on burn width and **(b)** estimation based on SD. It is applied for CSSR1.

AMTD
7, 9537–9571, 2014